Received: 11 January 2018 | Revised: 26 December 2018 | Accepted: 14 January 2019
DOI: 10.1002/we.2319

RESEARCH ARTICLE

WILEY

Do we really need rotor equivalent wind speed?

Wilfried G.J.H.M. Van Sark[1] | Henrik C. Van der Velde[1] | Jan P. Coelingh[2] | Wim A.A.M. Bierbooms[3]

[1] Utrecht University, Copernicus Institute of Sustainable Development, Princetonlaan 8a, 3584 CB Utrecht, The Netherlands

[2] Nuon, part of Vattenfall "BA Wind", PO Box 41920, 1009 DC Amsterdam, The Netherlands

[3] Faculty of Aerospace Engineering, Wind Energy Group, Delft University of Technology, PO Box 5058, 2600 GB Delft, The Netherlands

Correspondence
Wilfried van Sark, Utrecht University, Copernicus Institute of Sustainable Development, Princetonlaan 8a, 3584 CB, Utrecht, The Netherlands.
Email: w.g.j.h.m.vansark@uu.nl

Present Address
H.C. van der Velde, Nuon, part of Vattenfall "BA Wind," PO Box 41920, 1009 DC Amsterdam, The Netherlands

Abstract

The use of the rotor equivalent wind speed for determination of power curves and annual energy production for wind turbines is advocated in the second edition of the IEC 61400-12-1 standard. This requires the measurements of wind speeds at different heights, for which remote sensing equipment is recommended in addition to meteorological masts. In this paper, we present a theoretical analysis that shows that the relevance of the rotor equivalent wind speed method depends on turbine dimensions and wind shear regime. For situations where the ratio of rotor diameter and hub height is smaller than 1.8, the rotor equivalent wind speed method is not needed if the wind shear coefficient at the location of the wind turbine has a constant value between −0.05 and 0.4: in these cases, the rotor equivalent wind speed and the wind speed at hub height are within 1%. For complex terrains with high wind shear deviations are larger. The effect of non-constant wind shear exponent, ie, different wind shear coefficients for lower and upper half of the rotor swept area especially at offshore conditions is limited to also about 1%.

KEYWORDS

LiDAR, power curve, remote sensing, rotor equivalent wind speed, wind shear

1 | INTRODUCTION

Wind energy installed capacity has been increasing rapidly in the past decade to reach 539 GW worldwide at the end of 2017.[1] Expectations for further growth are high, and the terawatt level may be reached within the next decade.[2] Technology development has focused on cost reductions based on technological innovations, operation and maintenance optimization, mass production, and grid integration.[3-8] Commercial wind turbines with 6 to 7 MW rated capacity are available that have 156-m rotor diameter,[9] while designs of 10 MW turbines with >200-m rotor diameter have been presented.[10] These turbines are specifically designed to optimize energy yield at offshore locations.[11] As an example of wind turbine development in the Netherlands over the past 30 years, Figure 1 depicts hub height (H) and rotor diameter (D) in a scatterplot (total capacity of turbines shown is 3.5 GW, data from windstats[12]). The light gray area indicates where it holds that $\frac{3}{2}D \geq H \geq \frac{1}{2}D$. The dark gray area indicates nonphysical values: $H \leq \frac{1}{2}D$. A linear fit of the data shows that $H = 0.789\ D + 14.9$ m, with coefficient of determination $R^2 = 0.777$. Note, for most of the turbines, the ratio of rotor diameter and hub height is smaller than 1.5.

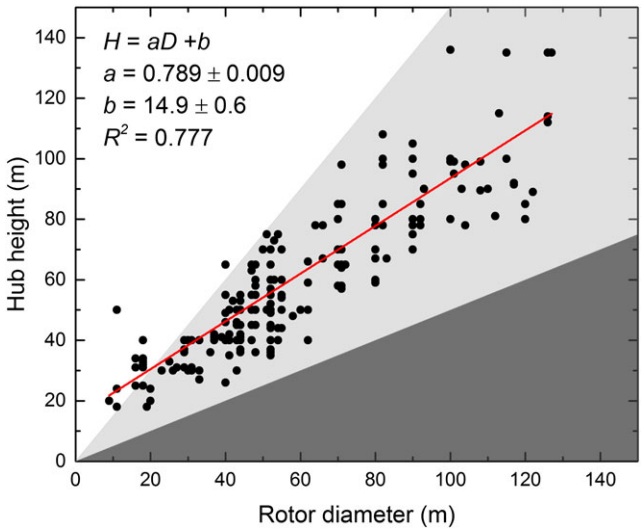

FIGURE 1 Development of rotor diameter and hub height for wind turbines installed in the Netherlands in the past 30 years totaling 3.5 GW (data from windstats[12]). The light gray area indicates where the ratio of rotor diameter and hub height is between 0.5 and 1.5; the dark gray area indicates nonphysical values [Colour figure can be viewed at wileyonlinelibrary.com]

With increasing size of wind turbines, stakes for good and accurate power curve measurements increase. The power curve estimates are used in combination with location specific annual wind speed distributions in order to estimate the annual amount of generated energy of a wind turbine and farm. In preconstruction analysis the power curve can be combined with the estimated or measured wind speed distribution to calculate the expected annual energy production of a wind turbine at a specific location. In postconstruction analysis, the contracted power curve can be compared with the actual (measured) power curve to determine whether the turbine is performing according to the guaranteed power curve.

Power curves for wind turbines are specified using the wind speed at hub height, according to the IEC 61400-12-1 standard.[13] However, since about 2005, new developments related to increased rotor diameters have led to the need to update this standard. Wind speed and wind direction at hub height are considered to become less representative for the wind conditions over the whole rotor area,[14,15] as wind speed at the lowermost height of the rotor may differ considerably from wind speed at the uppermost height. Also, these differences in wind speed may not be described by a single wind shear coefficient, which is used to describe wind speed as a function of height.

To address this issue, the rotor equivalent wind speed approach has been developed, where the wind speed at multiple heights within the rotor swept area is taken into account and translated to a representative (rotor equivalent) wind speed in order to provide more reliable and accurate power curves for large wind turbines.[16] A rotor swept area A should be subdivided in several horizontal segments (usually an uneven number, n_h), as shown in Figure 2. These segments (with areas A_i) are to be chosen such that the horizontal separation line between two segments lies exactly in the middle of two points at which the wind speed is to be measured. The second edition of the IEC standard[17] recommends power curves of turbines to be specified using the rotor equivalent wind speed u_{eq} instead of wind speed at hub height u_H.

In the development of the standard IEC 61400-12-1, Ed. 2,[17] the IEC Technical Committee 88 (TC88) on wind energy generation systems[18] was well aware[19] that in case of a constant wind shear coefficient, the difference of the rotor equivalent wind speed and the hub height wind speed is usually small. However, it was known from experiments[20,21] that in some cases the wind shear profile could not be well described by a constant wind shear coefficient. In those cases, the difference of rotor equivalent wind speed and the hub height wind speed could be significant. This is also why the standard IEC 61400-12-1, Ed. 2[17] does not allow the evaluation of rotor equivalent wind speed on the basis of a wind shear measurement only in the lower rotor half, while this would be sufficient in case of a constant wind shear coefficient over the total rotor height.

As a means to measure wind speeds at different heights, meteorological masts with anemometers higher and lower than hub height can be deployed as well as remote sensing devices. One such device is Light Detection And Ranging (LiDAR) technology, which has emerged due to its mobility and its ability of performing remote measurements up to heights of 200 m above ground level.[22-27] A LiDAR device measures the wind speed by analyzing the Doppler shift of an infrared laser beam reflected by aerosols.[22] It can be ground mounted or on the nacelle.[28] The second edition IEC standard[17] proposes to use a remote sensing device such as LiDAR to allow for measurements in situations, where a small meteorological mast is accompanying the LiDAR. The meteorological mast enables LiDAR validation and can measure fast fluctuations around the 10-minute mean wind speed (turbulence). Note that anemometers in fact are based on point measurements, while LiDAR is based on volume measurement.

LiDAR technology has been validated extensively: for flat terrain, the correlation between anemometer and LiDAR determined wind speed is very high.[22-26] At complex terrain, a LiDAR might perform insufficiently for wind speed measurements, due to the lack of horizontal homogeneity of the flow, which is assumed for the interpretation of LiDAR data[29] (it is therefore not recommended to be used in complex terrains[17]). The largest measurement uncertainties are related to, firstly, measuring at the intended measurement height, and, secondly, by interpolating the wind

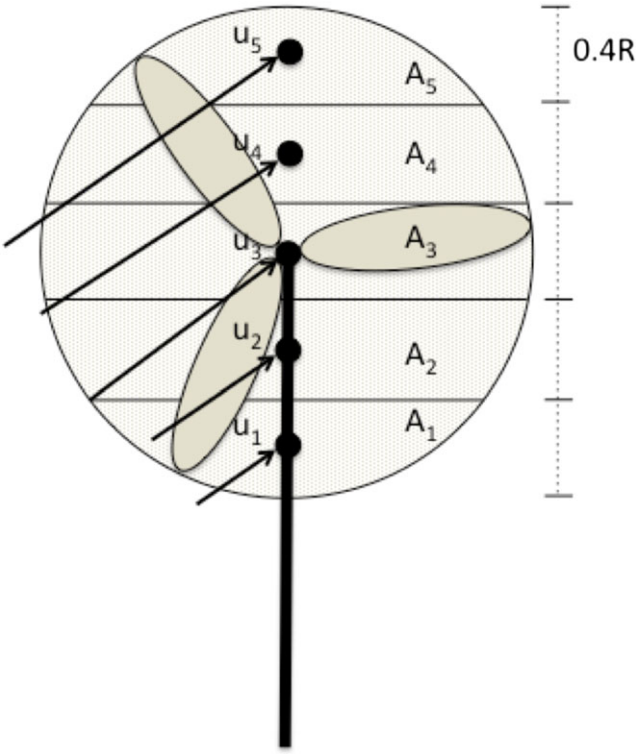

FIGURE 2 Illustration of determination of equivalent rotor wind speed, based on five different segments of the swept area *A1-A5* that are used to weigh the wind speeds at the center of the areas (adapted from Wagner et al[16]) [Colour figure can be viewed at wileyonlinelibrary.com]

speed from the measurements at some points along the measurement circle for which often the assumption is made that the wind speed is constant over that plane. For complex terrains, this is not a valid assumption. Generally, hardware issues and atmospheric conditions including rain, fog, and clouds influence uncertainties. A detailed analysis of factors influencing LiDAR measurements is provided by Lindelöw-Marsden.[30]

Multiple experimental studies have already analyzed the power performance test standards and conclude that the need of using the rotor equivalent may be questionable. Wagner et al[31] tested the rotor equivalent wind speed approach at one site for a 500-kW wind turbine (H = 36 m, D = 41 m) and found an insignificant influence of wind shear (changing wind speed with height). However, in an earlier study,[32] they found that using three or five different heights in the determination of rotor equivalent wind speed, the correlation between wind input and power output is improved. Wächter et al[33] measured the wind speed at hub height of a 5 MW turbine with a meteorological mast and a LiDAR at flat terrain and concluded that the power curves obtained after a 1-month measurement campaign were in good correspondence. Dupont et al[26] showed that the scatter of measurements around a fitted power curve is lower when using the rotor equivalent wind speed instead of the wind speed at hub height. Antoniou et al[34] concluded a yearlong measurement campaign with the notion that the rotor equivalent wind speed approach is to be recommended. Westerhellweg et al[25] showed that at an offshore site, the rotor equivalent wind speed approach improved the power performance test. Bardal et al[35] remarked that using the rotor equivalent wind speed approach scatter of the power curve should be reduced, while in their experiments using a 3 MW turbine during a 10-month measurement campaign, the rotor equivalent wind speed approach actually only marginally reduced the scatter in the power curve. Finally, we will show measurements of power curves for a 3.37 MW turbine (H = 98 m, D = 104 m) in a Dutch onshore wind park and will conclude that a rotor equivalent wind speed approach does not necessarily improve the uncertainty of the power curve measurement.

The purpose of this paper is to shed light on the potential value of using the rotor equivalent wind speed approach, while its use is recommended in the second edition IEC standard. We will do so based on an analytical description of wind shear effects on the rotor equivalent wind speed in dependence of the ratio of hub height and rotor diameter. Also, we will investigate the effects of using a single, constant wind shear coefficient, or of using two different values of the wind shear coefficient for the lower and upper half of the rotor swept area, respectively.

2 | THEORY

2.1 | Wind shear

Wind shear is defined as the difference in wind speed or direction between two layers of air in the atmosphere. Of relevance in this paper is the vertical wind shear. The height dependence of wind speed $u(h)$ is given as[36,37]

$$\frac{u(h)}{u_{ref}} = \left(\frac{h}{h_{ref}}\right)^{\alpha} \tag{1}$$

with α the constant wind shear coefficient, and the subscript "ref" referring to reference height (usually 10 m).

Another representation of the height dependence of the wind speed is based on using a roughness height parameter z_0, with displacement height d.[37-39] As in practical cases $d << h$, we can refine the definition:

$$\frac{u(h)}{u_{ref}} = \frac{\ln\left(\frac{h-d}{z_0}\right)}{\ln\left(\frac{h_{ref}-d}{z_0}\right)} \simeq \frac{\ln\left(\frac{h}{z_0}\right)}{\ln\left(\frac{h_{ref}}{z_0}\right)}. \tag{2}$$

While in the remainder of the paper, we will use Equation 1, we note that the wind shear coefficient α can be linked to the roughness length z_0 as follows[38]:

$$\alpha \simeq \frac{1}{\ln\left(\frac{\sqrt{h_{ref}h}}{z_0}\right)}. \tag{3}$$

Clearly, Equation 3 shows that α is height dependent, but usually a constant value is used as it only varies slightly with height. We do note though that non-constant wind shear coefficients have been reported: a ratio of wind shear coefficient of the upper part of the rotor swept area to the lower part is found to vary between 0.76[20] and ~2.[21]

The wind shear coefficient α is linked to the roughness of the terrain surrounding the wind turbine. For a smooth terrain, one considers that a constant wind shear coefficient α = 1/7 is a representative value; for a somewhat rougher terrain, α = 1/3.[40] In practice, the wind shear coefficient may vary between ~0.1 and 0.5,[21,41,42] or even 0.6,[43,44] as a result of different Pasquili weather stability classes A (unstable) to G (stable).[45,46] Lowest values are determined for class C (slightly unstable), while slightly larger values are found for classes A-B, and even higher for class D-G. Offshore conditions can be characterized by low values of α close to zero.[21,47] Even negative wind shear coefficients have been reported, which are due to nocturnal low level jets that appear typically 100 to 700 m above ground level.[48]

Using Equation 1, we can derive the ratio of the wind speeds at the top and the bottom of the rotor swept area:

$$\frac{u_{bottom}}{u_{ref}} = \left(\frac{H-\frac{1}{2}D}{H_{ref}}\right)^{\alpha} \text{ and } \frac{u_{top}}{u_{ref}} = \left(\frac{H+\frac{1}{2}D}{H_{ref}}\right)^{\alpha}. \tag{4}$$

It follows:

$$\frac{u_{top}}{u_{bottom}} = \left(\frac{H+\frac{1}{2}D}{H-\frac{1}{2}D}\right)^{\alpha} = \left(\frac{1+\frac{D}{2H}}{1-\frac{D}{2H}}\right)^{\alpha}. \tag{5}$$

Hence, for the turbine used by Bardal et al[35] (H = 92 m, D = 100.6 m), we calculate $u_{top}/u_{bottom} = 3.41^{\alpha}$, so that u_{top}/u_{bottom} = 1.19 for α = 1/7, and u_{top}/u_{bottom} = 1.51 for α = 1/3. For low wind shear coefficient values, the difference in wind speed over a length of 100 m is only ~20%, and it may be expected that the use of rotor equivalent wind speed may not be necessary, thus potentially avoiding the cost of additional wind speed measurement equipment.

Inspired by fitting data of Figure 1, but also from scaling laws presented elsewhere,[49] we assume

$$H = aD + b \tag{6}$$

with the obvious constraint that $D < 2H$, and for practical and operational reasons $D < 1.5H$. We derive

$$\frac{u_{top}}{u_{bottom}} = \left(\frac{a+\frac{1}{2}+\frac{b}{2D}}{a-\frac{1}{2}+\frac{b}{2D}}\right)^{\alpha} \tag{7}$$

which for $b<<D$ reduces to

$$\frac{u_{top}}{u_{bottom}} = \left(\frac{a+\frac{1}{2}}{a-\frac{1}{2}}\right)^{\alpha}. \tag{8}$$

Nijssen et al[49] suggested that for land based turbines, $a \approx 1$ and $b \approx 0$, so that Equation 8 could be used, while for offshore turbines $a \approx 0.5$ and b equals the maximum ocean wave height, so that Equation 7 needs to be used.

In the special case a = 1 (or H = D), Equation 8 reduces to $u_{top}/u_{bottom} = 3^{\alpha}$. Hence, for smooth terrain (α = 1/7), u_{top}/u_{bottom}= 1.17, and for rough terrain (α = 1/3), u_{top}/u_{bottom}= 1.44. For a = 0.5 and b = 10 m (which occurs at wind force of 10-11 Beaufort[50]), Equation 7 using D = 100 m gives $u_{top}/u_{bottom} = 11^{\alpha}$, and thus u_{top}/u_{bottom}= 1.41 for α = 1/7, and u_{top}/u_{bottom}= 2.22 for α = 1/3.

2.2 | Rotor equivalent wind speed

2.2.1 | Constant wind shear coefficient

The rotor equivalent wind speed u_{eq} is defined as (using Figure 2)

$$u_{eq} = \sqrt[3]{\sum_{i=1}^{n_h} \frac{A_i}{A} u_i^3} \tag{9}$$

where A_i is the area of the i-th segment, ie, the segment the wind speed u_i is representative for. Figure 2 shows the case for n_h = 5, where the difference in heights of each sector is equal (ie, 0.2D).

Appendix A elaborates on the calculation of the segment areas for three, five, seven, and nine segments. The five heights h_i at the center of the segment are defined as

$$h_i = H + \frac{1}{5}(i-3)D \qquad \text{for } i \in (1,\ 5) \tag{10}$$

based on the general form for odd number of segments n_h as given in Equation A2.

We derive the ratio of wind speed u_i at height h_i and the wind speed at hub height u_H (using Equations 1 and B2 for n_h = 5), using constant wind shear coefficient and setting hub height as reference height:

$$\frac{u_i}{u_H} = \left(\frac{h_i}{H}\right)^{\alpha} = \left(\frac{H + \frac{1}{5}(i-3)D}{H}\right)^{\alpha} = \left(1 + \frac{1}{5}(i-3)\frac{D}{H}\right)^{\alpha}. \tag{11}$$

Values of h_i and u_i/u_H are given in Table 1, in which also the relative areas A_1-A_5 are shown (for calculation, see Table A1 in Appendix A).

Using the definition of rotor equivalent wind speed (Equation 9), we derive, for n_h = 5:

$$\frac{u_{eq}}{u_H} = \sqrt[3]{\sum_{i=1}^{5} \frac{A_i}{A}\left(\frac{u_i}{u_H}\right)^3}. \tag{12}$$

This can be expanded to, using Equation 11,

$$\frac{u_{eq}}{u_H} = \sqrt[3]{\frac{A_1}{A}\left(1-0.4\frac{D}{H}\right)^{3\alpha} + \frac{A_2}{A}\left(1-0.2\frac{D}{H}\right)^{3\alpha} + \frac{A_3}{A} + \frac{A_4}{A}\left(1+0.2\frac{D}{H}\right)^{3\alpha} + \frac{A_5}{A}\left(1+0.4\frac{D}{H}\right)^{3\alpha}}. \tag{13}$$

For rough terrain (α = 1/3), it easily follows from Equation 13 and using Table 1 that u_{eq}/u_H = 1 for all D/H due to symmetry of the segment definition. Obviously, for α = 0 u_{eq}/u_H = 1, too. For α > 1/3, it holds that u_{eq}/u_H > 1, while for 0 < α < 1/3 it can be shown that u_{eq}/u_H < 1 (see Appendix B). Generic equations for arbitrary but uneven n_h can be found in Appendix B1.

TABLE 1 Values for h_i, u_i/u_H, and A_i/A as shown in Figure 2

i	h_i	$\frac{u_i}{u_H}$	$\frac{A_i}{A}$
1	H − 0.4D	$(1-0.4\frac{D}{H})^{\alpha}$	0.1424
2	H − 0.2D	$(1-0.2\frac{D}{H})^{\alpha}$	0.2312
3	H	1	0.2529
4	H + 0.2D	$(1+0.2\frac{D}{H})^{\alpha}$	0.2312
5	H + 0.4D	$(1+0.4\frac{D}{H})^{\alpha}$	0.1424

2.2.2 | Non-constant wind shear coefficient

In case the wind shear coefficient is not constant over the whole rotor area, the ratio u_{eq}/u_H may be affected. We assume that the wind shear coefficient at the lower and upper half of the rotor can be represented by α_L and α_U, respectively. We then can rewrite Equation (13) to

$$\frac{u_{eq}}{u_H} = \sqrt[3]{\frac{A_1}{A}\left(1-0.4\frac{D}{H}\right)^{3\alpha_L} + \frac{A_2}{A}\left(1-0.2\frac{D}{H}\right)^{3\alpha_L} + \frac{A_3}{A} + \frac{A_4}{A}\left(1+0.2\frac{D}{H}\right)^{3\alpha_U} + \frac{A_5}{A}\left(1+0.4\frac{D}{H}\right)^{3\alpha_U}}. \tag{14}$$

We relate the wind shear coefficients as follows: $r_\alpha = \alpha_U/\alpha_L$, and we then investigate for which value r_α it holds that $0.9 < u_{eq}/u_H < 1.1$ to show the effect of non-constant wind shear coefficient.

3 | EXPERIMENTS

3.1 | Wind turbine

A measurement campaign was organized at the 122 MW Princess Alexia wind park (52.29 N, 5.387 E) in the municipality of Zeewolde, the Netherlands, from 25 September 2015 until 2 January 2016. This site is characterized by flat terrain with open farmland, which is partly overgrown with small trees. Also, some farmhouses are situated within the site. The wind park is surrounded by other turbines to the North and West and surrounded by forest to the East and West. At the site, 36 Senvion 3.4 M104 wind turbines with a rated power of 3.37 MW are installed, with hub height of 98 m and rotor diameter of 104 m. It is successful in operation since September 2013. A detailed map with wind turbine locations is shown in Appendix C (Figure C1).

3.2 | Wind speed measurement

In order to measure wind speeds at different heights, a LiDAR system is installed next to a 98-m-high meteorological mast with anemometers. The meteorological mast is positioned next to the two most northwest situated wind turbines at two to four rotor diameters distance compliant with the IEC standard (see Appendix C, Figure C2). A ZephIR 300DM LiDAR system was used and set up at ground level next to the meteorological mast. In this way, wind speeds can be measured between 10 and 200-m height above ground level.[51] The ZephIR 300DM is a continuous wave Doppler LiDAR, and it requires the 1.55-μm IR beam to be focused using a telescope. The measurement height then can be adjusted using the focus of the telescope; however, this leads to height-dependent focus areas. The focus area is approximately 0.07 m at 10-m height and 7.70 m at 100-m height.[51]

The measurement heights for the LiDAR needed to calculate the rotor equivalent wind speed were chosen using IEC 61400-12-1 Edition 2,[17] based on dividing the rotor swept area in five segments (Figure 2). For the wind turbine under study here, the calculations are performed with a segment height of 20.8 m (=0.2D). Table 2 shows the heights at which wind speeds are measured by the LiDAR and meteorological mast and corresponding turbine dimensions.

TABLE 2 Used heights in LiDAR measurements

Height, m LiDAR	Used Heights		
	Meteorological mast	Rotor equivalent wind speed	Turbine
9			
37			
46	x		Lower tip
56.4		x	
77.2		x	
98	x	x	Hub
118.8		x	
139.6		x	
150			Upper tip
175			
200			

3.3 | Wind shear

From the measurements of wind speeds, the constant wind shear coefficient can be determined. After rewriting Equation 5, we find

$$\alpha = \ln\left(\frac{u_{top}}{u_{bottom}}\right) \ln^{-1}\left(\frac{1+\frac{D}{2H}}{1-\frac{D}{2H}}\right) \tag{15}$$

which allows calculation of the wind shear coefficient. For the turbine in our work (D = 104 m and H = 98 m), we arrive at $\alpha = 0.846 \ln(u_{top}/u_{bottom})$. Using wind speeds measured at all heights by the LiDAR, the wind shear coefficient actually is found by fitting data to Equation 1.

3.4 | Power and energy production

Data of power and wind speed were averaged over 10-minute time intervals and binned using 0.5 m/s intervals. Annual energy production was calculated by multiplying the binned distribution of wind speed with the power output at that wind speed (power curve).

4 | RESULTS

4.1 | Wind shear

For a number of large turbines, specifications are collected in Table 3. A range of values of D/H can be seen, as well as a range of power densities in W/m^2. Calculation of u_{top}/u_{bottom} for wind shear coefficient α (1/7, 1/3, 1/2) has been performed for turbine data in Table 3 using Equation 5, and these are plotted together with turbine data from Figure 1 as a function of D/H in Figure 3, where obviously D/H ranges from 0 to 2. The capacity of the wind turbines depicted in Figure 1 ranges from several kW to several MW and clearly spans a large range of D/H values. For values $D/H < 1$, the effects of the wind shear coefficient value on u_{top}/u_{bottom} are relatively small. The newer turbines of Table 3 show $D/H > 1$, except for the Enercon E-126/7.5 MW, and for those values, the effect of wind shear is considerable. Note that the D/H value for the Sway Turbine ST10 is extremely high, with the bottom height just 8 m above ground level, which may cause issues with high waves in offshore locations.

4.2 | Rotor equivalent wind speed

4.2.1 | Constant wind shear coefficient

The ratio of the rotor equivalent wind speed and the wind speed at hub height u_{eq}/u_H has been calculated using Equation 12 for a range of values of the wind shear coefficient α from −0.2 to +0.6, where a five-segmented swept area is used (Equation 11 and Table 1), see Figure 4A. As derived before, it holds that $u_{eq}/u_H = 1$ for all D/H and $\alpha = 1/3$. The variation in u_{eq}/u_H ranges from +3% to −1% only, also for the newer, larger turbines, for

TABLE 3 Specifications of some mostly large wind turbines (based on data from Wagner et al and Powertechnology[28,54])

Turbine	Rated Capacity, MW	Rotor Diameter, m	Hub Height, m	D/H	Top Height, m	Bottom Height, m	Swept Area, m^2	Power Density, W/m^2
SeaTitan 10 MW	10	190	125	1.520	220	30	28 353	353
Sway turbine ST10	10	164	90	1.822	172	8	21 124	473
Areva 8 MW	8	180					25 447	314
Vestas V164-9.5 MW	9.5	164	105	1.562	187	23	21 124	450
Enercon E-126/7.5 MW	7.5	127	135	0.941	198.5	71.5	12 668	592
Samsung S7.0-171	7	171	110	1.555	195.5	24.5	22 966	305
REpower 6.2 M152	6.2	152	124	1.226	200	48	18 146	342
REpower 6.2 M126	6.2	126					12 469	497
Siemens SWT-6.0-154	6	154					18 627	322
Haliade 150-6 MW	6	150					17 671	340
Sinovel SL6000	6	128					12 868	466
Senvion 3.4 M104	3.37	104	98	1.061	150	46	8495	397
Nordtank0.5	0.5	41	36	1.139	56.5	15.5	1320	379

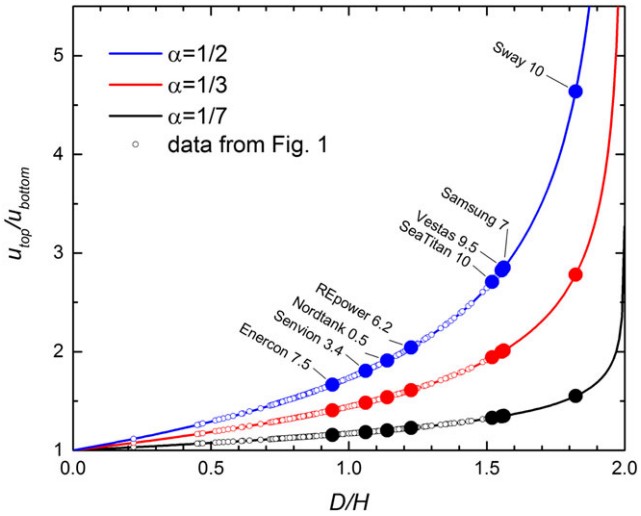

FIGURE 3 Ratio u_{top}/u_{bottom} as a function of D/H for three values of wind shear coefficient α (1/7, 1/3, 1/2). Solid lines are calculated using Equation 5, small open symbols correspond to data from Figure 1, and large solid symbols correspond to data from Table 3 [Colour figure can be viewed at wileyonlinelibrary.com]

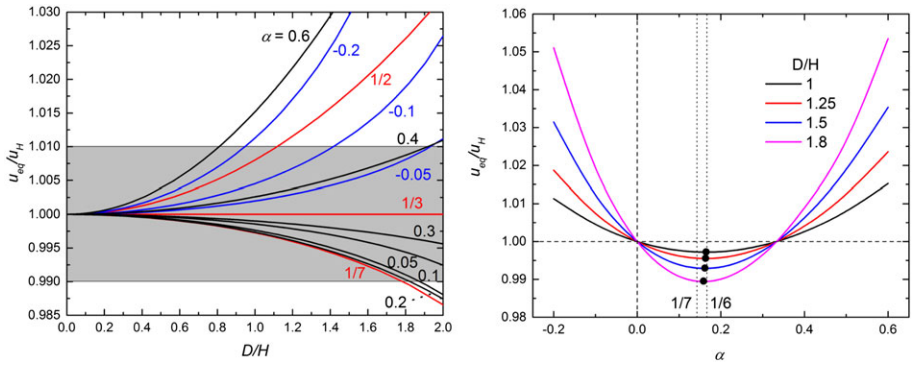

FIGURE 4 A, Ratio u_{eq}/u_H as a function of D/H for values of wind shear coefficient α ranging from −0.2 to +0.6 calculated with Equation 12. The gray shaded area denotes a + 1% to −1% range in u_{eq}/u_H; B, ratio u_{eq}/u_H as a function of α for 1 < D/H < 1.8 [Colour figure can be viewed at wileyonlinelibrary.com]

values of the wind shear coefficient between −0.1 and + 0.5 and the full realistic D/H range. The gray area in Figure 4A shows for which combination of α and D/H the ratio u_{eq}/u_H is within ±1%.

It can be seen that for values of $0 \leq \alpha \leq 1/3$ the rotor equivalent wind speed is smaller than the wind speed at hub height. This compares well with a study showing that for values of $0 < \alpha < \frac{1}{3}$, the rotor equivalent wind speed was up to 0.3% smaller than the wind speed at hub height (for a turbine with H = 92 m, D = 100.6 m)[35]; hence, using the wind speed at hub height would overestimate generated power, albeit slightly. For $-0.2 < \alpha < 0$ and $\frac{1}{3} < \alpha < 0.6$, this situation is reversed. Closer inspection of the dependence of u_{eq}/u_H on α for values of $\frac{D}{H} \geq 1$ as shown in Figure 4B reveals that a minimum in u_{eq}/u_H occurs for $\alpha \approx \frac{1}{6}$, where the location of the minimum is shifting toward $\alpha \approx \frac{1}{7}$ for increasing values of D/H. Clearly, the ratio u_{eq}/u_H < 1% for $\frac{D}{H} \leq 1.8$ and values of $0 < \alpha < \frac{1}{3}$.

We note that at very high wind shear exponents the rotor equivalent wind speed is larger than the wind speed at hub height. In this case, the angle of attack of the aerofoils along the blade will change a lot over a rotor revolution and as a consequence the induction factor as well as the lift-to-drag ratio will not be optimal. In order to obtain a first-order estimate of this effect simulations have been done with the aeroelastic code BLADED 4.6 for a generic 5 MW wind turbine. Unsteady effects like stall hysteresis and dynamic inflow are taken into account. For a wind shear coefficient of 0.5, this leads to a reduction in power output, at a hub wind speed of 10 m/s, of about 5%, rather than an expected increase. A possible way to mitigate this effect is to design special aerofoils with an extended drag bucket. Clearly, further research is recommended in this field.

4.2.2 | Non-constant wind shear coefficient

Figure 5 shows a contour plot of u_{eq}/u_H as a function of a_L on the x-axis and r_a on the y-axis, for D/H = 1. It is clear that the minimum value of u_{eq}/u_H equals about 0.97, and the maximum is about 1.12, while values higher than 1.05 times u_{eq}/u_H are found for a_L > 0.5 and a_U/a_L > 1.5, which are not found often in realistic conditions. We note that for other values of D/H > 1, the contour plots look very similar, while the range of values, especially the maximum value of u_{eq}/u_H, clearly differs. Minimum and maximum values of u_{eq}/u_H are shown in Table 4. For offshore conditions, wind shear values are usually small, and as a consequence the effect of a non-constant wind shear coefficient on u_{eq}/u_H is around ±1%.

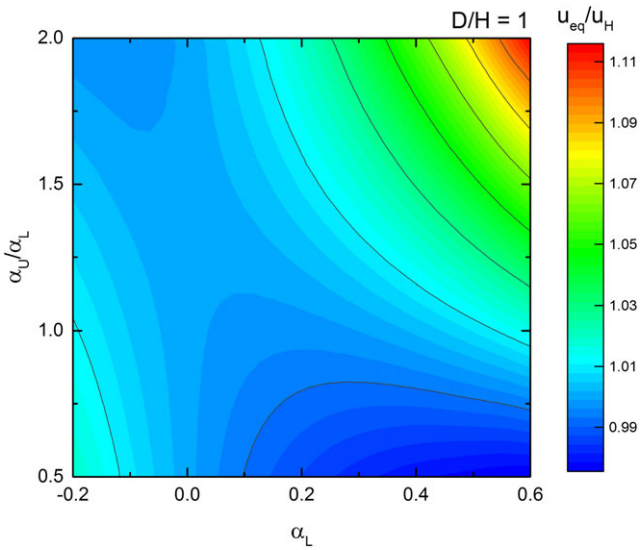

FIGURE 5 Contour plot of u_{eq}/u_H as a function of α_L on the x-axis and r_α on the y-axis, for D/H = 1. The minimum value of u_{eq}/u_H equals about 0.97, and the maximum is about 1.12, while values higher than 1.05 times u_{eq}/u_H are found for α_L > 0.5 and r_α > 1.5.% [Colour figure can be viewed at wileyonlinelibrary.com]

TABLE 4 Maximum(*at* a_U/a_L = 2) and minimum (*at* a_U/a_L = 0.5) values of u_{eq}/u_H for four values of D/H; these occur at a_L = 0.6

$\frac{D}{H}$	Minimum	Maximum
1.0	0.976	1.1160
1.25	0.972	1.1600
1.5	0.970	1.210
1.8	0.968	1.275

4.3 | Experimental

From the 3-month measurement period of wind characteristics at the site, a mean wind speed of 7.94 m/s at hub height is found, with prevailing wind direction from the southwest, see Figure C3 in Appendix C. Fitting the data to a two-parameter Weibull function[40,42] yields shape parameter k = 2.26 and scale parameter c = 8.97 m/s. Note that for a three times longer measurement campaign (3 February 2015 to 2 January 2016), using the meteorological mast only, we have found k = 2.18 and scale parameter c = 7.80 m/s, with mean wind speed of 6.91 m/s. While the shape parameter is similar, the scale parameter is lower, due to lower wind speeds in summer and spring. The prevailing wind direction is similar as well.

The comparison of the wind speeds measured using the LiDAR and the meteorological mast at two heights is shown in Figure 6. The correlation is excellent, as was expected, while at lower wind speeds around the cut-in wind speed of the turbine, the LiDAR shows somewhat higher wind speeds than the meteorological mast at 46 m height.

The linear regression of the wind speed at hub height and rotor equivalent wind speed shows that there is little difference (Figure 7): the slope of the fit shows that rotor equivalent wind speed is ~0.2% smaller than the wind speed at hub height. This is also reflected in the power curve (Figure 8): the relative power curve differences are lower than 2% except for low wind speeds. Higher differences around the cut-in wind speed (3 m/s) are hardly relevant for energy production. Estimation of the annual energy production following procedures in the IEC standard revealed that the use of the rotor equivalent wind speed leads to ~0.5% lower annual yield than using the wind speed at hub height (not shown here), which is to be expected given the power curve results.

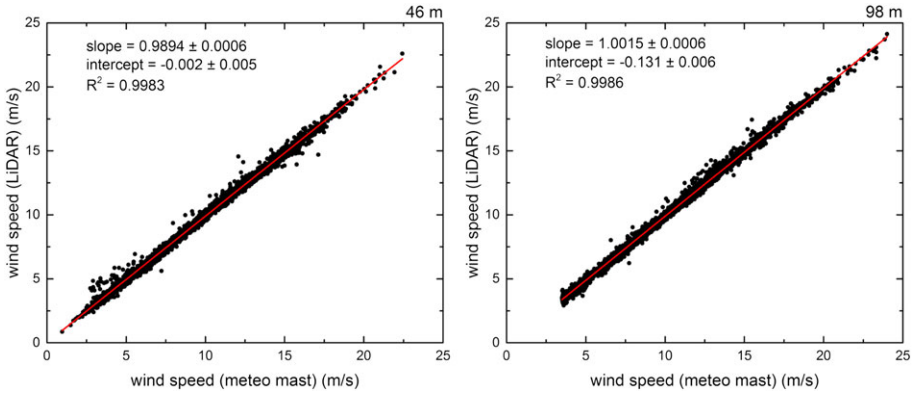

FIGURE 6 Comparison of wind speed measured with LiDAR and meteorological mast at two heights (46 and 98 m) [Colour figure can be viewed at wileyonlinelibrary.com]

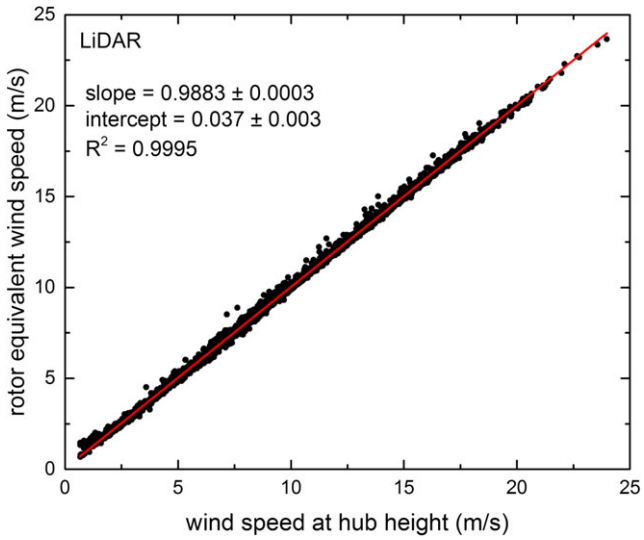

FIGURE 7 Linear regression of rotor equivalent wind speed and wind speed at hub height measured with LiDAR [Colour figure can be viewed at wileyonlinelibrary.com]

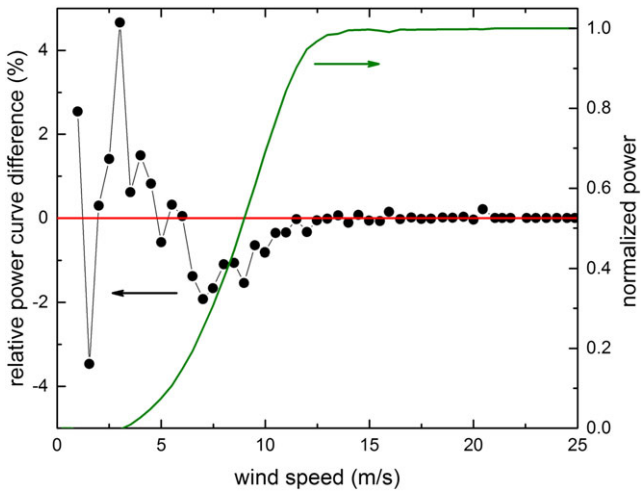

FIGURE 8 Relative power curve difference (left axis) using rotor equivalent wind speed and wind speed at hub height, and power curve versus rotor equivalent wind speed (normalized to rated power) (right axis). Wind speeds are measured with LiDAR [Colour figure can be viewed at wileyonlinelibrary.com]

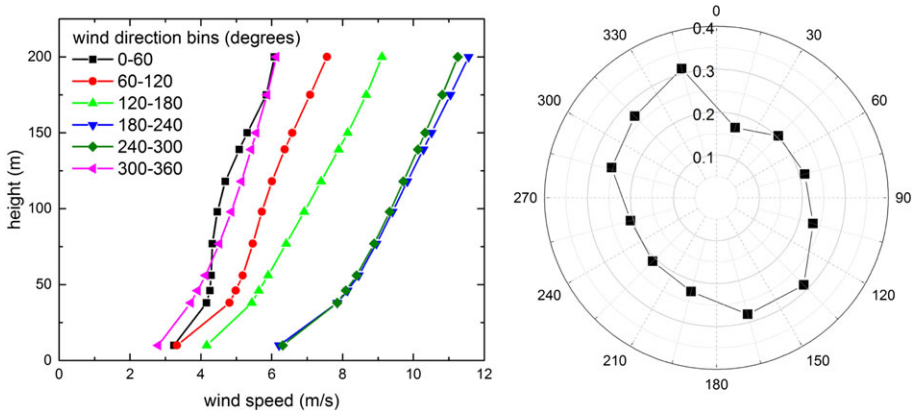

FIGURE 9 A, Wind speed profiles for different wind directions (60 degrees bins); B, derived wind shear coefficient (30 degrees bins) [Colour figure can be viewed at wileyonlinelibrary.com]

The wind shear coefficient was determined by fitting the wind profiles measured using LiDAR. Figure 9A shows these profiles as a function of wind direction (binned per 60 degrees). Note that the direction 0-60 degrees is the direction from the closest wind turbine of the park, and clear wake effects on the wind profile can be seen. Figure 9B shows the wind direction-dependent wind shear coefficient to vary between 0.08 and 0.3, depending on the wind direction (binned per 30 degrees), which can be expected given the open terrain. As said, the lowest values between the North and East wind directions are due to wake effects from the wind park on the measurements. The measured wind shear coefficient values with the value of D/H of the used turbine lead to minimal effects on the power curve when comparing rotor equivalent wind speed and wind speed at hub height, perfectly in line with calculations as shown in Figure 4.

The accuracy of the height measurement of the LiDAR may influence the wind speed. In the appendix of Smith et al,[22] the probe length (full width half maximum, FWHM) at 50 m is shown to be ~4 m (8%), at 100 m ~15 m (15%), and at 200 m ~60 m (22%). The LiDAR equipment used in our experiments has improved FWHM probe length of 7.7 m at 100-m height, or 7.7%.[51] Note, as the FHWM probe length is not equal to the height error of the center of the probe volume, a realistic uncertainty linked to the probe length can be obtained by integrating over the probe lengths, and the resulting measured wind speed should be compared with the wind speed at the center of the probe volume. The resulting measurement error then is around 0.5%.

Another issue may be the fact that the probe lengths of two adjacent selected heights for which the LiDAR should measure wind speed may be overlapping, which may be the case for large heights. A curve like the one in Figure 9A should include errors in the measurement points, and these should also be included in the determined wind shear coefficient. However, as this issue is more prominent at large heights, fitting results are not expected to be influenced much.

Finally, fitting the height versus wind speed curves leads to an error in the value of the constant wind shear coefficient. We found typical fitting errors of 3% to 6% for all wind directions in our experiment, except for the 0-60 degrees wind direction, which is affected by wake effects, where we find a fitting error of 13%. Also, we note that in determining the wind shear coefficient using only wind speeds at the lower half of the rotor, we find identical wind shear coefficients when fitting wind speeds for the full rotor area, except for, again, the direction 0-60 degrees. This shows that in the experimental case studied here, a constant wind shear coefficient is found over the whole rotor area.

5 | CONCLUSION AND RECOMMENDATIONS

This paper has presented a theoretical analysis and experimental results to address the use of the rotor equivalent wind speed as advocated in the second edition of the IEC 61400-12-1 standard. The use of remote sensing technology such as LiDAR is recommended in order to determine wind speeds at various heights in an easy and cheap manner. As was shown before, LiDAR wind speed measurements correlate excellently with wind speed measurements using anemometers in meteorological masts. With new, large wind turbines being installed and designed, the rotor equivalent wind speed method is recommended. However, in this paper, we show that the relevance of this method depends on turbine dimensions, ie, the ratio of rotor diameter and hub height, as well as on the wind shear coefficient at the location of the wind turbine. Calculations and experiments at the wind park in this paper show that the rotor equivalent wind speed method may not be always needed and determination of the wind speed at hub height by means of the meteorological mast is sufficient. In fact, up to realistically large $\frac{D}{H} \leq 1.8$ and $-0.05 < \alpha < 0.4$, the ratio u_{eq}/u_H is within ±1% of unity. The effect of non-constant wind shear coefficient especially at offshore conditions is limited to also about 1%.

We therefore recommend to first estimate the wind shear coefficient at a particular site and depending on the result decide on the investment in a LiDAR system next to an already installed meteorological mast. For wind shear coefficient values out of the range $-0.05 < \alpha < 0.4$, the rotor

equivalent wind speed method is recommended. This thus pertains to more complex terrains, or terrains with more vegetation. This recommendation also holds for non-constant wind shear coefficients at these locations. Interestingly, for large offshore turbines with large D/H, the rotor equivalent wind speed method may not be needed at all as typical wind shear coefficient values are ~0.1. However, for operational reasons, the fact that the LiDAR instrument is mobile, it can be very useful, especially in onshore wind farms in determination of wind profiles at various locations in the wind farm to validate single turbine performance in conjunction with a measured wind profile. Finally, if one is concerned about reducing uncertainty in power curves, financial benefits may outweigh investment in LiDAR equipment.

ACKNOWLEDGEMENTS

We would like to thank Tim Besseling and Hidde Seidel of Nuon/Vattenfall for assistance with LiDAR measurements and wind farm access. Henrik Van der Velde gratefully acknowledges the hospitality of Nuon/Vattenfall during his research work. We further thank anonymous reviewers who through their comments have contributed considerably to improve the quality of the paper.

ORCID

Wilfried G.J.H.M. Van Sark https://orcid.org/0000-0002-4738-1088

REFERENCES

1. Global Wind Energy Council. Global wind report annual market Update 2017. 2018.
2. Navigant Consulting. World Wind Energy Market Update 2015 International Wind Energy Development: 2015-2019. Copenhagen, Denmark; 2015.
3. Chang J, Ummels BC, van Sark WGJHM, den Rooijen HPGM, Kling WL. Economic evaluation of offshore wind power in the liberalized Dutch power market. *Wind Energy*. 2009;12(5):507-523. https://doi.org/10.1002/we.334
4. Zugno M, Jónsson T, Pinson P. Trading wind energy on the basis of probabilistic forecasts both of wind generation and of market quantities. *Wind Energy*. 2013;16(6):909-926. https://doi.org/10.1002/we.1531
5. Barthelmie RJ, Pryor SC. Potential contribution of wind energy to climate change mitigation. *Nat Clim Chang*. 2014;4(8):684-688. https://doi.org/10.1038/nclimate2269
6. Van Sark WGJHM, Schepers JG, Van Wees JDAM. The growing role of photovoltaic solar, wind and geothermal energy as renewables for electricity generation. In: Dewulf J, De Meester S, Alvarenga RAF, eds. *Sustainability Assessment of Renewables-Based Products: Methods and Case Studies*. Chichester, UK: Wiley; 2016:19-36.
7. Colmenar-Santos A, Perera-Perez J, Borge-Diez D, DePalacio-Rodríguez C. Offshore wind energy: a review of the current status, challenges and future development in Spain. *Renew Sustain Energy Rev*. 2016;64:1-18. https://doi.org/10.1016/j.rser.2016.05.087
8. Voormolen JA, Junginger HM, van Sark WGJHM. Unravelling historical cost developments of offshore wind energy in Europe. *Energy Policy*. 2016;88:435-444. https://doi.org/10.1016/j.enpol.2015.10.047
9. Siemens. Offshore Direct Drive Wind Turbine SWT-6.0-154.2016. http://www.siemens.com/global/en/home/markets/wind/turbines/swt-6-0-154.html. Accessed November 5, 2016.
10. Schepers JG, Ceyhan O, Savenije FJ, et al. AVATAR: AdVanced Aerodynamic Tools for lArge Rotors. In: *33rd ASME Wind Energy Symposium*. Kissimmee: American Society of Mechanical Engineers; 2015.
11. Offshore Wind Programme Board. Cost Reduction Monitoring Framework 2015.2016. https://ore.catapult.org.uk/our-knowledge-areas/knowledge-standards/knowledge-standards-projects/cost-reduction-monitoring-framework/. Accessed November 5, 2016.
12. Bosch, Van Rijn. Statistics on wind energy. 2016. www.windstats.nl. Accessed November 5, 2016.
13. International Electrotechnical Commission. IEC 61400-12-1, Wind turbines—Part 12-1: power performance measurements of electricity producing wind turbines, Edition 1.; 2005.
14. European Wind Energy Association. Wind energy—the facts: a guide to the technology, economics and future of wind power; 2009. http://www.wind-energy-the-facts.org.
15. Wharton S, Lundquist JK. Atmospheric stability affects wind turbine power collection. *Environ Res Lett*. 2012;7(1):014005.
16. Wagner R, Courtney J, Gottschall J, Lindelöw-Marsden P. Accounting for the speed shear in wind turbine power performance measurement. *Wind Energy*. 2011;11(8):993-1004. https://doi.org/10.1002/we.509.
17. International Electrotechnical Commission. IEC 61400-12-1, Wind turbines—Part 12-1: power performance measurements of electricity producing wind turbines, 2nd ed. 2017.
18. IEC Technical Committee 88 (TC88) Wind energy generation systems. https://www.iec.ch/tc88
19. Anonymous. Review comment.
20. Bratton DC, Womeldorf CA. The wind shear exponent: comparing measured against simulated values and analyzing the phenomena that affect the wind shear. In: *Proceedings of the ASME 2011 5th International Conference on Energy Sustainability ES2011*. 2011:ES2011–54.
21. Wharton S, Lundquist JK. Assessing atmospheric stability and its impacts on rotor-disk wind characteristics at an onshore wind farm. *Wind Energy*. 2012;15(4):525-546. https://doi.org/10.1002/we.483
22. Smith DA, Harris M, Coffey AS, et al. Wind lidar evaluation at the Danish wind test site in Høvsøre. *Wind Energy*. 2006;9(1–2):87-93. https://doi.org/10.1002/we.193

23. Mann J, Cariou J-P, Courtney MS, et al. Comparison of 3D turbulence measurements using three staring wind lidars and a sonic anemometer. *IOP Conf Ser Earth Environ Sci*. 2008;1:012012.
24. Peña A, Hassager CB, Gryning S-E, Courtney M, Antoniou I, Mikkelsen T. Offshore wind profiling using light detection and ranging measurements. *Wind Energy*. 2009;12(2):105-124.
25. Westerhellweg A Canadillas B, Beeken A, Neumann T. One year of lidar measurements at FINO1-platform: comparison and verification to met-mast data. In: Proceedings of the 10th German Wind Energy Conference DEWEK. 2010:1–5.
26. Dupont E, Lefranc Y, Soutlier L, Koulibaly D. Detailed analysis of uncertainty reduction on power curve determination using lidar measurements. In: Proceedings of EWEA2012. 2012:16–19.
27. Simley E, Angelou N, Mikkelsen T, Sjöholm M, Mann J, Pao LY. Characterization of wind velocities in the upstream induction zone of a wind turbine using scanning continuous-wave lidars. *J Renew Sustain Energy*. 2016;8(1):013301. https://doi.org/10.1063/1.4940025
28. Wagner R, Pedersen TF, Courtney M, Antoniou I, Davoust S, Rivera RL. Power curve measurement with a nacelle mounted lidar. *Wind Energy*. 2014;17:1441-1453. https://doi.org/10.1002/we.1643
29. Bingöl F, Mann J, Foussekis D. Conically scanning lidar error in complex terrain. *Meteorol Z*. 2009;18(2):189-195.
30. Lindelöw-Marsden P. *UpWind D1. Uncertainties in wind assessment with LIDAR*. Roskilde, Denmark: Risø National Laboratory; 2009 http://orbit.dtu.dk/fedora/objects/orbit:82842/datastreams/file_5113517/content.
31. Wagner R, Cañadillas B, Clifton A, et al. Rotor equivalent wind speed for power curve measurement—comparative exercise for IEA wind annex 32. *J Phys Conf Ser*. 2014;524:012108.
32. Wagner R, Antoniou L, Pedersen SM, Courtney MS, Jørgensen HE. The influence of the wind speed profile on wind turbine performance measurements. *Wind Energy*. 2009;12(4):348-362.
33. Wächter M, Gottschall J, Rettenmeier A, Peinke J. Power curve estimation using lidar measurements. In: Proceedings of the EWEA European Wind Energy Conference.; 2009:4473–4477.
34. Antoniou L, Pedersen SM, Enevoldsen PB. Wind shear and uncertainties in power curve measurement and wind resources. *Wind Eng*. 2009;33(5):449-468.
35. Bardal LM, Sætran LR, Wangsness E. Performance test of a 3MW wind turbine—effects of shear and turbulence. *Energy Procedia*. 2015;80:83-91.
36. Hansen MOL. *Aerodynamics of Wind Turbines*. Second ed. London: Earthscan; 2008.
37. Emeis S. *Wind Energy Meteorology*. 2nd ed. Cham, Switzerland: Springer International Publishing AG; 2018.
38. Wieringa J. Updating the Davenport roughness classification. *J Wind Eng Ind Aerodyn*. 1992;41–44(1-3):357-368.
39. Wieringa J. Representative roughness parameters for homogeneous terrain. *Bound-Lay Meteorol*. 1993;63(4):323-363.
40. Twidell J, Weir T. *Renewable Energy Resources*. 3rd ed. London: Routledge; 2015.
41. Sisterson DL, Hicks BB, Coulter RL, Wesely ML. Difficulties in using power laws for wind energy assessment. *Sol Energy*. 1983;31(2):201-204.
42. Rehman S, Al-Abbadi NM. Wind shear coefficients and their effect on energy production. *Energ Conver Manage*. 2005;46(15-16):2578-2591. https://doi.org/10.1016/j.enconman.2004.12.005.
43. Hanafusa T, Lee CB, Lo AK. Dependence of the exponent in power law wind profiles on stability and height interval. *Atmos Environ*. 1986;20(10):2059-2066.
44. Gualtieri G. Atmospheric stability varying wind shear coefficients to improve wind resource extrapolation: a temporal analysis. *Renew Energy*. 2016;87:376-390. https://doi.org/10.1016/j.renene.2015.10.034
45. Pasquill F. The estimation of the dispersion of windborne material. *Meteorol Mag*. 1961;90(10):33-49.
46. Venkatram A. An examination of the Pasquill-Gifford-turner dispersion scheme. *Atmos Environ*. 1996;30(8):1283-1290.
47. Peña A, Gryning S-E. Charnock's roughness length model and non-dimensional wind profiles over the sea. *Bound-Lay Meteorol*. 2008;128(2):191-203. https://doi.org/10.1007/s10546-008-9285-y.
48. Gutierrez W, Araya G, Kiliyanpilakkil P, Ruiz-Columbrie A, Tutkun M, Castillo L. Structural impact assessment of low level jets over wind turbines. *J Renew Sustain Energy*. 2016;8(2):023308. https://doi.org/10.1063/1.4945359.
49. Nijssen RPL, Zaaijer MB, Bierbooms WAAM, Van Kuik GAM, Van Delft DR V, Van Holten T. The application of scaling rules in up-scaling and marinisation of a wind turbine. In: Proceedings European Wind Energy Conference and Exhibition (EWEC).; 2001:619–622.
50. National Oceanic and Atmospheric Administration. Beaufort Wind Force Scale. http://oceanservice.noaa.gov/education/yos/resource/JetStream/ocean/beaufort_max.htm. Accessed November 5, 2016.
51. ZephIR. https://www.zephirlidar.com/support/tech-specs/. Accessed November 1, 2016.
52. Weisstein EW. Circular segment. MathWorld—A Wolfram Web Resour 2016. http://mathworld.wolfram.com/CircularSegment.html.
53. Abramowitz M, Stegun IA. *Handbook of Mathematical Functions with Formulas, Graphs, and Mathematical Tables*. Ninth ed. New York: Dover Publications; 1970.
54. Powertechnology.com. The world's 10 biggest wind turbines. 2014. http://www.power-technology.com/features/featurethe-worlds-biggest-wind-turbines-4154395. Accessed November 4, 2016.

How to cite this article: Van Sark WGJHM, Van der Velde HC, Coelingh JP, Bierbooms WAAM. Do we really need rotor equivalent wind speed? *Wind Energy*. 2019;22:745–763. https://doi.org/10.1002/we.2319

APPENDIX A

CALCULATION OF SEGMENT AREAS

The calculation of the rotor equivalent wind speed is based on the segmentation of the swept area A in an uneven number of different segments A_1-A_n, which are used to weigh the wind speeds at the center of the areas. As example, we show the calculation for five segments A_1-A_5 as illustrated in Figure 2. We use a procedure for the calculation of the area of a circular sector, as depicted as the shaded area in Fig. A1.[52] This circular sector has an upper boundary of an arc of length s and a lower boundary of a chord with length a, which makes an angle $\theta < \pi$ and a height h. The circle has radius R, and r is the height of the triangle of sides of length R and a. Thus, $R = h + r$, $s = R\theta$, and $r = R\cos\left(\frac{1}{2}\theta\right)$.

The general solution for area of the circular sector is[52]

$$A = R^2 \cos^{-1}\left(\frac{R-h}{R}\right) - (R-h)\sqrt{2Rh - h^2}. \tag{A1}$$

Referring to Figure 2, areas A_1 and A_5 can be directly calculated with Equation A1. For area A_1, a circular segment with chord a_1 and height $h = 0.4R$ is used. For area A_2, a circular segment with chord a_2 being the upper boundary of area A_2 is calculated first. This equals $A_1 + A_2$, and subsequently area A_1 is subtracted from that. Area A_3 then is calculated using $A_1 + A_2 + \frac{1}{2}A_3 = \frac{1}{2}\pi R^2$. A similar approach is used for area A_4 and A_5. The final result is given in Table A1, where A_i is given relative to the swept area A. Note that these values are slightly different from some of the ones reported by Wagner et al[31] in an exercise with several experts for a case of a turbine with hub height of 80 m and a rotor diameter of 100 m ($D/H = 1.25$).

For convenience, also the results for three, seven, and nine segments are shown in Tables A2, A3, and A4, respectively, which have been calculated following a similar approach.

Using the segmentation of rotor swept area, we can write the general equation for odd n_h as

$$h_i = H + \frac{1}{n_h}\left(i - \left(\frac{n_h + 1}{2}\right)\right)D. \tag{A2}$$

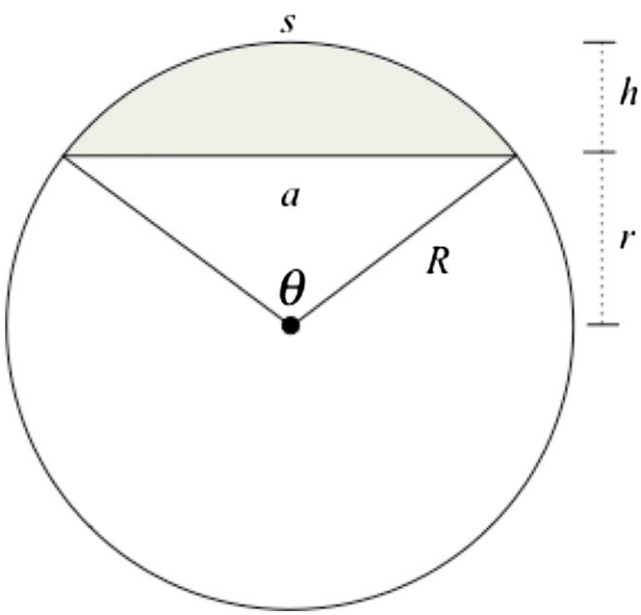

FIGURE A1 Circular sector area calculation [Colour figure can be viewed at wileyonlinelibrary.com]

TABLE A1 Calculated areas A_1-A_5 of Figure 2. Values are rounded to four digits after the decimal point

i	A_i	$\frac{A_i}{A}$
1	$R^2(\cos^{-1}(0.6) - 0.48)$	0.1424
2	$R^2\left(\cos^{-1}(0.2) - 0.2\sqrt{0.96}\right) - A_1$	0.2312
3	$\pi R^2 - (A_1 + A_2 + A_4 + A_5)$	0.2529
4	$R^2\left(\cos^{-1}(0.2) - 0.2\sqrt{0.96}\right) - A_5$	0.2312
5	$R^2(\cos^{-1}(0.6) - 0.48)$	0.1424

TABLE A2 Calculated areas A_1-A_3

i	A_i	$\frac{A_i}{A}$
1	$R^2\left(\cos^{-1}\left(\frac{1}{3}\right) - \frac{2\sqrt{2}}{9}\right)$	0.2918
2	$\pi R^2 - (A_1 + A_3)$	0.4164
3	$R^2\left(\cos^{-1}\left(\frac{1}{3}\right) - \frac{2\sqrt{2}}{9}\right)$	0.2918

TABLE A3 Calculated areas A_1-A_7

i	A_i	$\frac{A_i}{A}$
1	$R^2\left(\cos^{-1}\left(\frac{5}{7}\right) - \frac{10\sqrt{6}}{49}\right)$	0.0876
2	$R^2\left(\cos^{-1}\left(\frac{3}{7}\right) - \frac{6\sqrt{10}}{49}\right) - A_1$	0.1481
3	$R^2\left(\cos^{-1}\left(\frac{1}{7}\right) - \frac{4\sqrt{3}}{49}\right) - A_2 - A_1$	0.1736
4	$\pi R^2 - (A_1 + A_2 + A_3 + A_5 + A_6 + A_7)$	0.1813
5	$R^2\left(\cos^{-1}\left(\frac{1}{7}\right) - \frac{4\sqrt{3}}{49}\right) - A_6 - A_7$	0.1736
6	$R^2\left(\cos^{-1}\left(\frac{3}{7}\right) - \frac{6\sqrt{10}}{49}\right) - A_7$	0.1481
7	$R^2\left(\cos^{-1}\left(\frac{5}{7}\right) - \frac{10\sqrt{6}}{49}\right)$	0.0876

TABLE A4 Calculated areas A_1-A_9

i	A_i	$\frac{A_i}{A}$
1	$R^2\left(\cos^{-1}\left(\frac{7}{9}\right)-\frac{28\sqrt{2}}{81}\right)$	0.0607
2	$R^2\left(\cos^{-1}\left(\frac{5}{9}\right)-\frac{10\sqrt{14}}{81}\right)-A_1$	0.1047
3	$R^2\left(\cos^{-1}\left(\frac{1}{3}\right)-\frac{\sqrt{8}}{9}\right)-A_2-A_1$	0.1263
4	$R^2\left(\cos^{-1}\left(\frac{1}{9}\right)-\frac{4\sqrt{5}}{81}\right)-A_3-A_2-A_1$	0.1376
5	$\pi R^2-(A_1+A_2+A_3+A_4+A_6+A_7+A_8+A_9)$	0.1412
6	$R^2\left(\cos^{-1}\left(\frac{1}{9}\right)-\frac{4\sqrt{5}}{81}\right)-A_7-A_8-A_9$	0.1376
7	$R^2\left(\cos^{-1}\left(\frac{1}{3}\right)-\frac{\sqrt{8}}{9}\right)-A_8-A_9$	0.1263
8	$R^2\left(\cos^{-1}\left(\frac{5}{9}\right)-\frac{10\sqrt{14}}{81}\right)-A_9$	0.1047
9	$R^2\left(\cos^{-1}\left(\frac{7}{9}\right)-\frac{28\sqrt{2}}{81}\right)$	0.0607

APPENDIX B

CALCULATION OF ROTOR EQUIVALENT WIND SPEED

B.1 | Constant wind shear coefficient

From the definition of rotor equivalent wind speed, it follows

$$u_{eq}=\sqrt[3]{\sum_{i=1}^{n_h}\frac{A_i}{A}u_i^3}=u_H\sqrt[3]{\sum_{i=1}^{n_h}\frac{A_i}{A}\left(\frac{u_i}{u_H}\right)^3}\quad\Rightarrow\quad\frac{u_{eq}}{u_H}=\sqrt[3]{\sum_{i=1}^{n_h}\frac{A_i}{A}\left(\frac{u_i}{u_H}\right)^3}. \tag{B1}$$

Thus, we need to determine the ratio u_i/u_H, which can be expressed in h_i/H.

Using Equation 1 and Equation A2, we derive

$$\frac{u_i}{u_H}=\left(\frac{h_i}{H}\right)^\alpha=\left(\frac{H+\frac{1}{n_h}\left(i-\left(\frac{n_h+1}{2}\right)\right)D}{H}\right)^\alpha=\left(1+\frac{1}{n_h}\left(i-\left(\frac{n_h+1}{2}\right)\right)\frac{D}{H}\right)^\alpha. \tag{B2}$$

The ratio u_{eq}/u_H can then be derived as follows:

$$\frac{u_{eq}}{u_H}=\sqrt[3]{\sum_{i=1}^{n_h}\frac{A_i}{A}\left(\frac{u_i}{u_H}\right)^3}=\sqrt[3]{\sum_{i=1}^{n_h}\frac{A_i}{A}\left(1+\frac{1}{n_h}\left(i-\left(\frac{n_h+1}{2}\right)\right)\frac{D}{H}\right)^{3\alpha}}. \tag{B3}$$

Figure 4 depicts u_{eq}/u_H, using $n_h = 5$ for various values of $-0.2 < \alpha < 0.6$.

An analytical example for the five-segment case of Figure 2 is the following:

$$\frac{u_{eq}}{u_H}=\sqrt[3]{\frac{A_1}{A}\left(1-0.4\frac{D}{H}\right)^{3\alpha}+\frac{A_2}{A}\left(1-0.2\frac{D}{H}\right)^{3\alpha}+\frac{A_3}{A}+\frac{A_4}{A}\left(1+0.2\frac{D}{H}\right)^{3\alpha}+\frac{A_5}{A}\left(1+0.4\frac{D}{H}\right)^{3\alpha}} \tag{B4}$$

with $0<\frac{D}{H}<2$, $0<\alpha<1$, $A_1=A_5$, $A_2=A_4$, and $\sum_{i=1}^{5}A_i=A$.

The special case $\alpha=\frac{1}{3}$ yields $u_{eq}=u_H$, for all $\frac{D}{H}$, because of $\sum_{i=1}^{5}A_i=A$. In fact, this holds for all n_h.

For $\alpha = \frac{2}{3}$, we find after some algebra:

$$\frac{u_{eq}}{u_H} = \sqrt[3]{\frac{A_1}{A}\left(1-0.4\frac{D}{H}\right)^2 + \frac{A_2}{A}\left(1-0.2\frac{D}{H}\right)^2 + \frac{A_3}{A} + \frac{A_4}{A}\left(1+0.2\frac{D}{H}\right)^2 + \frac{A_5}{A}\left(1+0.4\frac{D}{H}\right)^2} = \sqrt[3]{1+\left(0.32\frac{A_1}{A}+0.08\frac{A_2}{A}\right)\left(\frac{D}{H}\right)^2} > 1. \tag{B5}$$

Hence, $u_{eq} > u_H$, for all $\frac{D}{H}$.

For $\alpha = \frac{1}{6}$, we find

$$\frac{u_{eq}}{u_H} = \sqrt[3]{\frac{A_1}{A}\sqrt{1-0.4\frac{D}{H}} + \frac{A_2}{A}\sqrt{1-0.2\frac{D}{H}} + \frac{A_3}{A} + \frac{A_4}{A}\sqrt{1+0.2\frac{D}{H}} + \frac{A_5}{A}\sqrt{1+0.4\frac{D}{H}}} = \sqrt[3]{\frac{A_1}{A}\left(\sqrt{1-0.4\frac{D}{H}} + \sqrt{1+0.4\frac{D}{H}}\right) + \frac{A_2}{A}\left(\sqrt{1-0.2\frac{D}{H}} + \sqrt{1+0.2\frac{D}{H}}\right) + \frac{A_3}{A}}. \tag{B6}$$

Using Taylor expansions of $\sqrt{1+x}$ and $\sqrt{1-x}$ for x < 1,[53] we find

$$\begin{aligned}\sqrt{1-x} + \sqrt{1+x} &= \left(1 - \frac{x}{2} - \frac{x^2}{8} - \frac{x^3}{16} + \ldots\right) + \left(1 + \frac{x}{2} - \frac{x^2}{8} + \frac{x^3}{16} + \ldots\right) \\ &= 2 - \frac{x^2}{4} - O(x^4).\end{aligned} \tag{B7}$$

Substitution in Equation B6 leads to

$$\frac{u_{eq}}{u_H} = \sqrt[3]{\frac{A_1}{A}\left(2 - \frac{\left(0.4\frac{D}{H}\right)^2}{4} - \ldots\right) + \frac{A_2}{A}\left(2 - \frac{\left(0.2\frac{D}{H}\right)^2}{4} - \ldots\right) + \frac{A_3}{A}}. \tag{B8}$$

As $\frac{2A_1}{A} + \frac{2A_2}{A} + \frac{A_3}{A} = 1$, for all $c\frac{D}{H}$, with $c < 0.5$ and $\frac{D}{H} < 2$, it follows $u_{eq} < u_H$.

The minimum of Equations 12 and B4 for $n_h = 5$ can be derived. We first need to find the derivative and equate this to zero:

$$\frac{d\left(\sqrt[3]{\sum_{i=1}^{5}\frac{A_i}{A}\left(1+\frac{1}{5}(i-3)\frac{D}{H}\right)^{3\alpha}}\right)}{d\alpha} = \frac{\sum_{i=1}^{5}\frac{A_i}{A}\left(1+\frac{1}{5}(i-3)\frac{D}{H}\right)^{3\alpha}\ln\left(1+\frac{1}{5}(i-3)\frac{D}{H}\right)}{\left[\sum_{i=1}^{5}\frac{A_i}{A}\left(1+\frac{1}{5}(i-3)\frac{D}{H}\right)^{3\alpha}\right]^{2/3}} = 0. \tag{B9}$$

We need to solve for α, thus

$$\begin{aligned}&\sum_{i=1}^{5}\frac{A_i}{A}\left(1+\frac{1}{5}(i-3)\frac{D}{H}\right)^{3\alpha}\ln\left(1+\frac{1}{5}(i-3)\frac{D}{H}\right) = 0 \\ &\Rightarrow \frac{A_1}{A}\left(1-\frac{2D}{5H}\right)^{3\alpha}\ln\left(1-\frac{2D}{5H}\right) + \frac{A_2}{A}\left(1-\frac{1D}{5H}\right)^{3\alpha}\ln\left(1-\frac{1D}{5H}\right) + \frac{A_4}{A}\left(1+\frac{1D}{5H}\right)^{3\alpha}\ln\left(1+\frac{1D}{5H}\right) + \frac{A_5}{A}\left(1+\frac{2D}{5H}\right)^{3\alpha}\ln\left(1+\frac{2D}{5H}\right) = 0 \\ &\Rightarrow \frac{A_1}{A}\left[\left(1-\frac{2D}{5H}\right)^{3\alpha}\ln\left(1-\frac{2D}{5H}\right) + \left(1+\frac{2D}{5H}\right)^{3\alpha}\ln\left(1+\frac{2D}{5H}\right)\right] + \frac{A_2}{A}\left[\left(1-\frac{1D}{5H}\right)^{3\alpha}\ln\left(1-\frac{1D}{5H}\right) + \left(1+\frac{1D}{5H}\right)^{3\alpha}\ln\left(1+\frac{1D}{5H}\right)\right] = 0\end{aligned}$$

where we note that $A_1 = A_5$ and $A_2 = A_4$. The term with A_3 is zero, due to the natural logarithm value at $i = 3$. Taking values for D/H ranging from 1.0 to 1.8 (as used in Figure 4), we can solve for α, and results are given in Table B1. Note that these values are somewhat smaller than 1/6. Also, α decreases slightly with increasing D/H. These minima are also shown in Figure 4B.

TABLE B1 Values of α for minima of u_{eq}/u_H for $1 \le \frac{D}{H} \le 1.8$

$\frac{D}{H}$	α
1.0	0.164772
1.25	0.163542
1.5	0.161824
1.8	0.158751

B.2 | Roughness length

The ratio u_i/u_H can also be derived as follows using the roughness length z_0 as in Equation 3:

$$\frac{u_i}{u_H} = \frac{\ln\left(\frac{h_i}{z_0}\right)}{\ln\left(\frac{H}{z_0}\right)}. \tag{B10}$$

The ratio u_{eq}/u_H can then be derived as follows (with h_i defined in Equation A2):

$$\frac{u_{eq}}{u_H} = \sqrt[3]{\sum_{i=1}^{n_h} \frac{A_i}{A}\left(\frac{u_i}{u_H}\right)^3} = \sqrt[3]{\sum_{i=1}^{n_h} \frac{A_i}{A}\left(\frac{\ln\left(\frac{h_i}{z_0}\right)}{\ln\left(\frac{H}{z_0}\right)}\right)^3} = \frac{1}{\ln\left(\frac{H}{z_0}\right)}\sqrt[3]{\sum_{i=1}^{n_h} \frac{A_i}{A}\left(\ln\left(\frac{h_i}{z_0}\right)\right)^3}. \tag{B11}$$

APPENDIX C

WIND PARK LOCATION AND MEASUREMENTS

The location of the 122 MW Princess Alexia wind park (52.29 N, 5.387 E) is shown in Figure C1, the red shaded area. The wind park is designed with three rows of 12 Senvion 3.4 M104 wind turbines. The open farmland of the area contains some farmhouses and small trees, as well as many other wind turbines that do not belong to the wind park. The meteorological mast is positioned next to the two most northwest situated wind turbines at two to four rotor diameters distance, see Figure C2. Wind speed and wind rose distributions from the measurement campaign of 25 September 2015 until 2 January 2016 are shown in Figure C3.

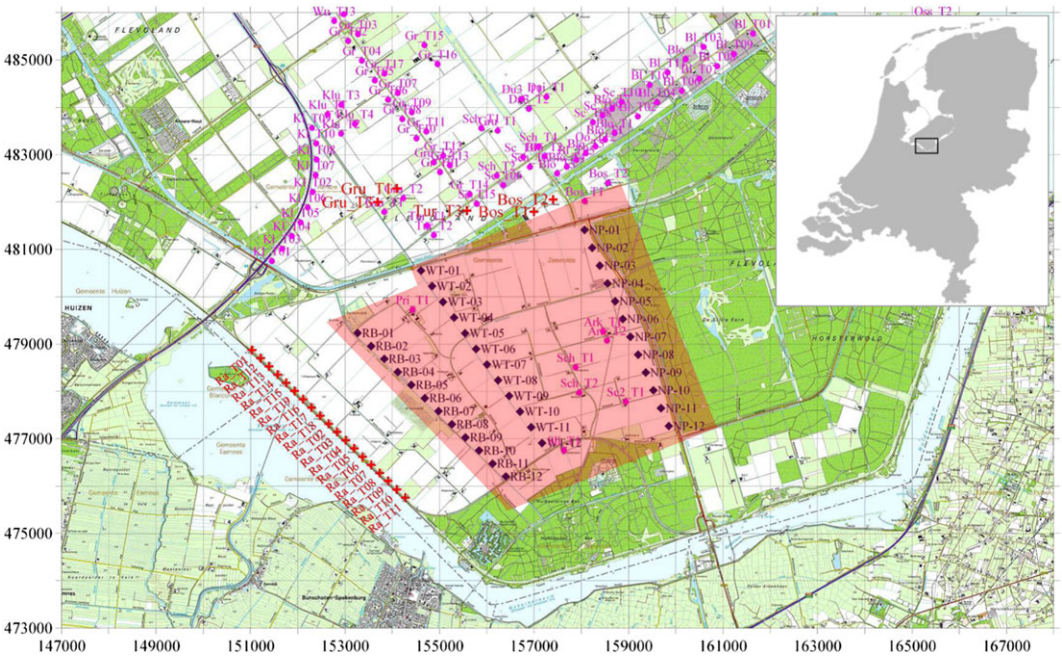

FIGURE C1 Location of the Princess Alexia site in the province of Flevoland (see inset for a country perspective). The red area in the middle shows three rows of 12 wind turbines. The LiDAR is installed next to the most northern turbine of the most left row (see also Figure C2 for detail). The *x* and *y* axes are given in meters. Red plusses and purple dots represent other turbine sites [Colour figure can be viewed at wileyonlinelibrary.com]

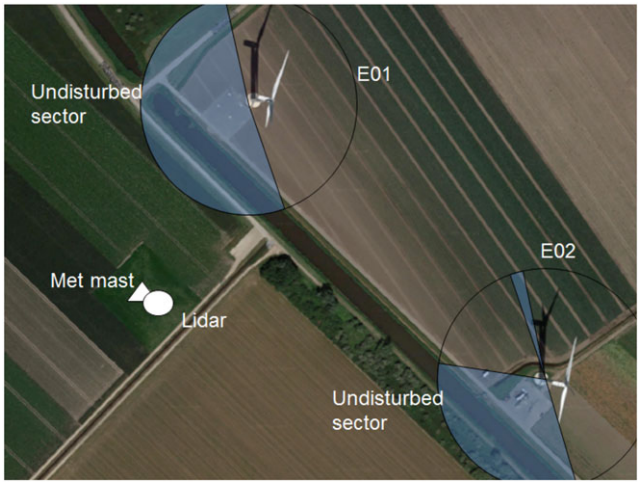

FIGURE C2 Detailed location of meteorological mast, LiDAR, and two wind turbines [Colour figure can be viewed at wileyonlinelibrary.com]

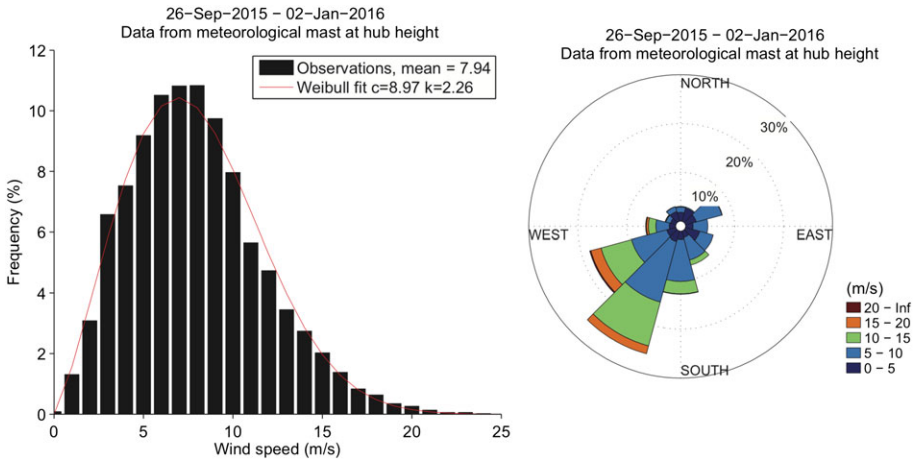

FIGURE C3 Wind speed distribution and wind rose, at hub height. Wind speed distribution at hub height can be fitted with a Weibull distribution with k = 2.26 and c = 8.97 m/s, with mean wind speed of 7.94 m/s [Colour figure can be viewed at wileyonlinelibrary.com]